Journal of Alloys and Compounds 831 (2020) 154878

Contents lists available at ScienceDirect

Journal of Alloys and Compounds

journal homepage: http://www.elsevier.com/locate/jalcom

# High-performance microwave dielectric composite ceramics sintered at low temperature without sintering-aids

Rui Peng [a], Yuanxun Li [a, b, *], Yongcheng Lu [a], Yanru Yun [d], Wei Du [a], Zhihua Tao [a], Bin Liao [c]

[a] State Key Laboratory of Electronic Thin Films and Integrated Devices, University of Electronic Science and Technology of China, Chengdu, 610054, China
[b] Jiangxi Guochuang Industrial Park Development Co., Ltd, Ganzhou, 341000, China
[c] Ganzhou DPT Technology Co., Ltd, Ganzhou, 341000, China
[d] Jincheng College of Sichuan University, Chengdu, 611731, China

ARTICLE INFO

*Article history:*
Received 16 December 2019
Received in revised form
19 March 2020
Accepted 19 March 2020
Available online 24 March 2020

*Keywords:*
Low dielectric constant
LTCC
Dielectric properties
Disconnection model
Sintering kinetics

ABSTRACT

(1-x)$Li_2(Mg_{0.96}Ni_{0.04})SiO_4$+x$LiZn_{0.93}Co_{0.07}PO_4$ composite ceramics were synthesised through solid-state reaction, and their sintering kinetics, microstructure and microwave dielectric properties were investigated. The perfect disconnection model was applied to explain the variation in grain growth with different x values and sintering temperatures. X-ray diffraction, scanning electron microscopy, thermomechanical analysis and network analysis were used to determine the macro and micro properties of the composite ceramics. Results showed that $LiZn_{0.93}Co_{0.07}PO_4$ ceramic could promote grain growth and grain boundary modification, due to the different levels of shear stress and free energy density of the Si-rich and P-rich phases. The shrinkage onset point of the composite ceramics was adjusted to achieve full densification at 900 °C. The peak microwave dielectric properties are $\varepsilon_r = 5.78$, $Q \times f = 48{,}168$ GHz at 16 GHz and $\tau_f = -44.7$ ppm/°C when x = 0.5, sintering temperature is 900 °C and relative density is 96.1%. Therefore, mixing $LiZn_{0.93}Co_{0.07}PO_4$ (pre-sintered) and $Li_2(Mg_{0.96}Ni_{0.04})SiO_4$ (pre-sintered) ceramics is a feasible synthesis method for microwave dielectric materials with excellent sintering and dielectric properties.



## 1. Introduction

Low temperature co-fired ceramic (LTCC) technology is a packaging method that facilitates large-scale 3D integration of passive devices instead of patching on the surface and can be widely applied in military and civilian products, such as aerospace and smart homes [1]. Generally, the embedded electrode of LTCC is Ag, which has a melting point of 961 °C [2]. However, 900 °C is preferable in manufacturing to maintain the quality of the printed circuit. Adding glass and multicomponent oxides with a low melting point is a popular method to achieve low temperature densification, but the deterioration of dielectric properties is the usual effect of densification at a relatively low temperature [1,3,4]. Therefore, realizing low temperature sintering without additives negatively affecting microwave properties is a project worth studying.

The low signal transmission delay, high signal quality and stable thermal stability could be achieved by materials with extremely low $\varepsilon_r$, high $Q \times f$ and near-zero $\tau_f$ value [5]. Silicate (with low dielectric constant and stable thermal stability) and phosphate (with low sintering temperature and high $Q \times f$ value) have recently attracted the interest of researchers [3,6,7]. In our previous study, the dielectric properties of $Li_2(Mg_{0.96}Ni_{0.04})SiO_4$ (LMNS) ceramics are improved as $\varepsilon_r = 5.69$, $Q \times f = 28{,}448$ GHz at 16 GHz, $\tau_f = -15.3$ ppm/°C sintered at 1150 °C, and those of $LiZn_{0.93}Co_{0.07}PO_4$ (LZCP) ceramics are $\varepsilon_r = 5.43$, $Q \times f = 35{,}446$ GHz at 15 GHz, $\tau_f = -77.4$ ppm/°C sintered at 850 °C [6,7]. However, these two materials can be further enhanced. The sintering temperature of LMNS is excessively high to fulfil the requirements of LTCC, and its $Q \times f$ value should be improved. Besides, the absolute $\tau_f$ value of LZCP should be decreased. LZCP has low $\varepsilon_r$, high $Q \times f$ value and low sintering temperature, whereas LMNS has small absolute $\tau_f$ value. Hence, adding the LZCP ceramic into the LMNS ceramic results in

* Corresponding author. State Key Laboratory of Electronic Thin Films and Integrated Devices, University of Electronic Science and Technology of China, Chengdu, 610054, China.
*E-mail address:* liyuanxun@uestc.edu.cn (Y. Li).

https://doi.org/10.1016/j.jallcom.2020.154878
0925-8388/

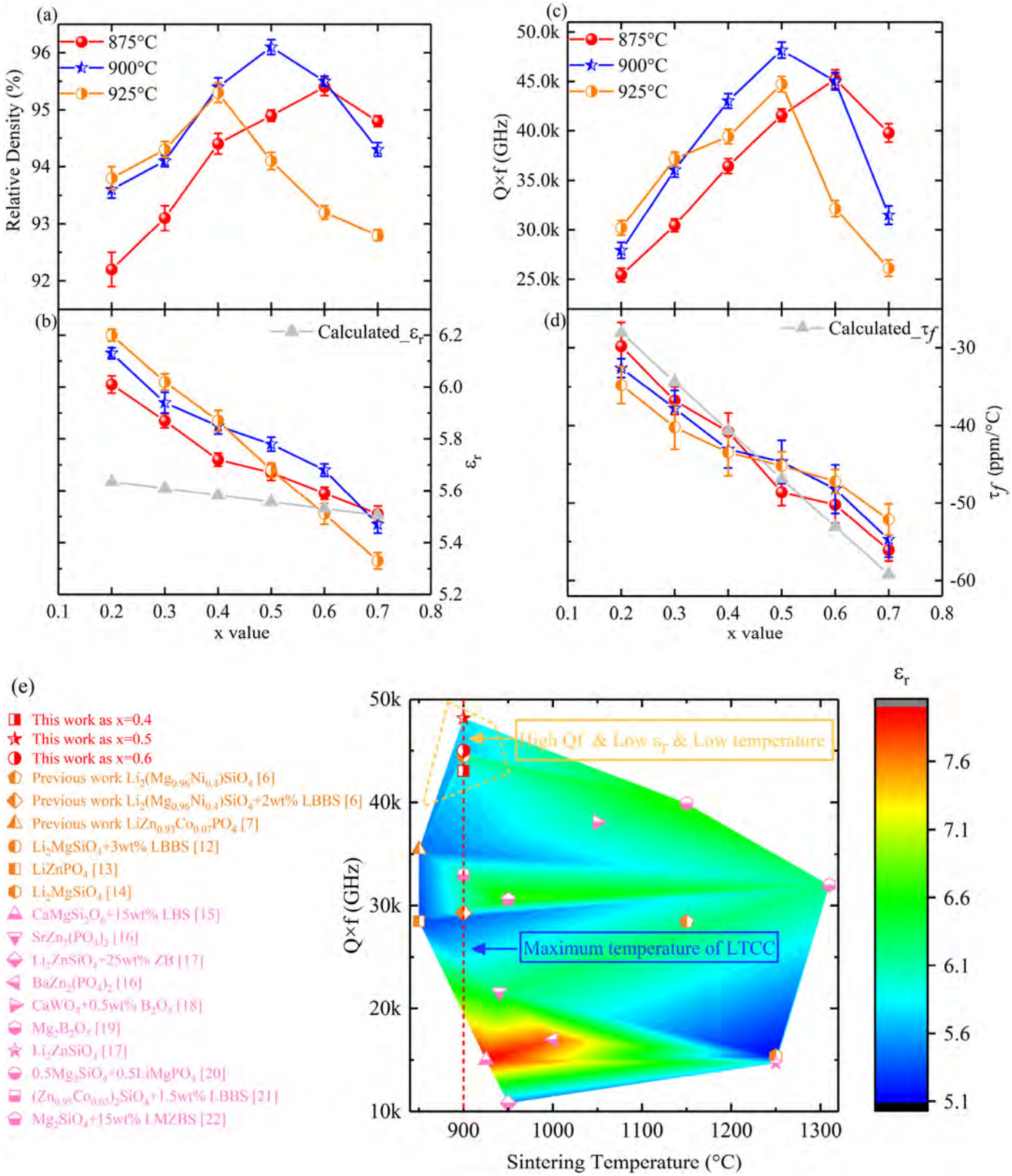


**Fig. 1.** Relative density (a), $\varepsilon_r$ (b), $Q\times f$ (c), and $\tau_f$ (d) values of the (1-x)LMNS + xLZCP (x = 0.2–0.7) ceramics sintered at 875-925 °C for 4 h; summary of dielectric and sintering properties of various ceramics (e).

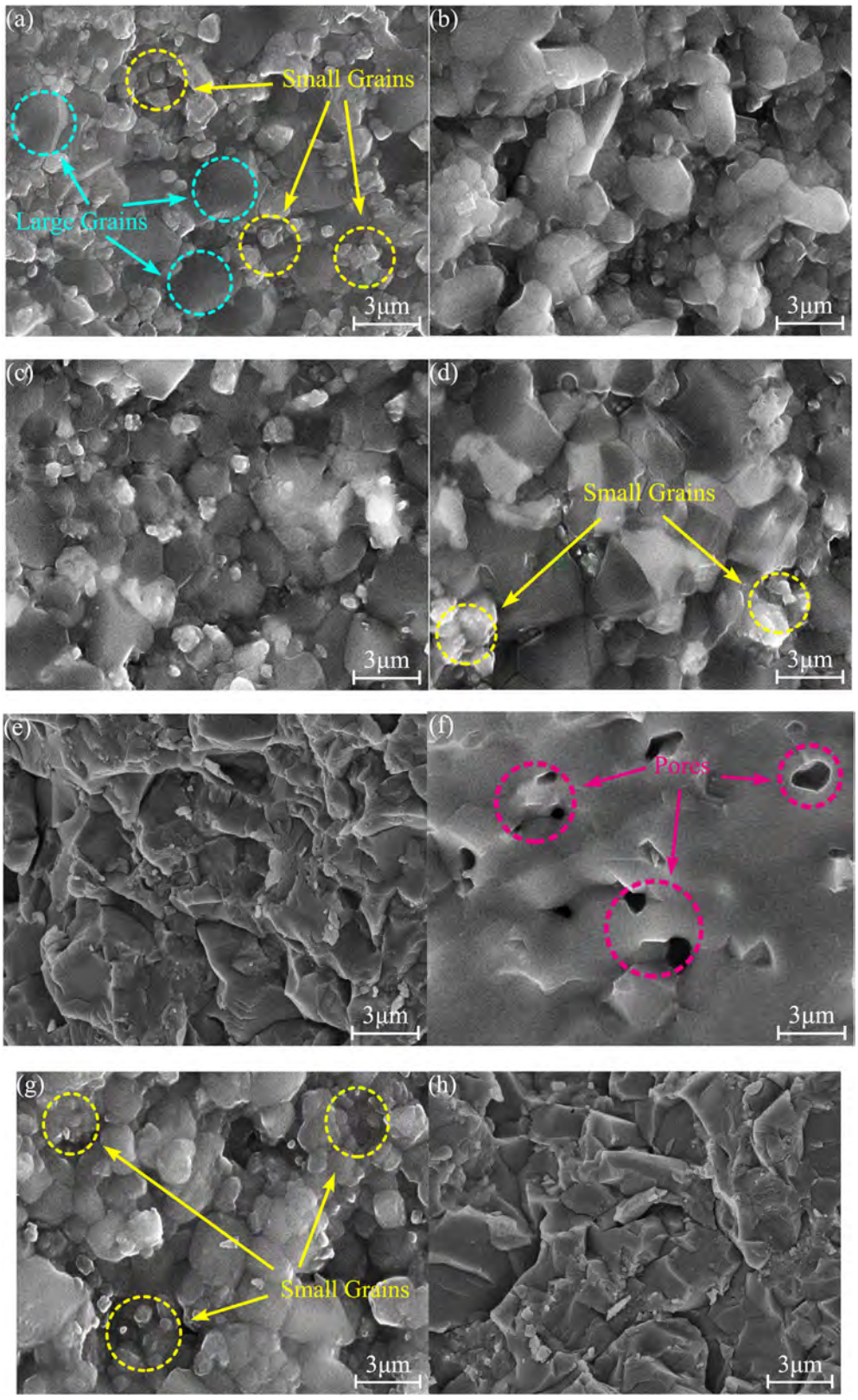


**Fig. 2.** SEM micrographs of (1-x)LMNS + xLZCP, x = 0.2 (a), x = 0.3 (b), x = 0.4 (c), x = 0.5 (d), x = 0.6 (e), x = 0.7 (f) ceramics sintered at 900 °C for 4 h, x = 0.5 sintered at 875 °C for 4 h (g), and x = 0.5 sintered at 925 °C for 4 h (h).

many benefits. Firstly, LZCP ceramic has relatively low densification temperature and therefore could act as the medium of heat transfer. The low temperature sintering of LMNS ceramic could be realized without sintering-aids which could deteriorate the microwave properties. Secondly, the LMNS + LZCP ceramic could be equipped with higher $Q \times f$ value and lower $\varepsilon_r$ compared with those of the LMNS ceramic. The thermal stability of the composite ceramics would be better than that of the LZCP ceramic. To date, the sintering kinetics and microwave dielectric properties of (1-x) LMNS + xLZCP (x = 0.2−0.7) composite ceramics have not been researched.

In this study, (1-x)LMNS + xLZCP (x = 0.2−0.7) composite ceramics were synthesised via solid-state reaction. The sintering kinetics, microscopic mechanism of grain boundaries (GBs), phase composition and microwave dielectric properties of these composite materials were investigated. A novel modification method for sintering, microstructure and microwave dielectric properties was also proposed. The findings of this study may be useful in the field of structural and functional ceramics.

## 2. Experimental procedures

High-purity powders of $Li_2CO_3$ (99.5%), MgO (99%), NiO (99.5%), ZnO (99.5%), $Co_2O_3$ (99.5%), $NH_4H_2PO_4$ (99%) and $SiO_2$ (99.5%) (all of these analytical purity powders are from Chron Chemicals Co. Ltd, Chengdu, China) were chosen as the raw materials to prepare the composite ceramics through conventional solid-state reaction. According to molar ratio, LMNS and LZCP ceramics were pre-milled separately in a nylon pot filled with zirconia balls for 24 h. The milled slurry was dried and pre-sintered for 4 h. The calcination temperature is 830 °C for LMNS ceramic and 650 °C for LZCP ceramic. The pre-sintered powders were remilled in accordance with the x value of (1-x)LMNS + xLZCP (x = 0.2−0.7, mole ratio) in distilled water for 24 h and subsequently dried. The powders were ground, mixed with 5 wt% of polyvinyl alcohol and pressed into disks (12 mm in diameter and 6 mm in thickness), which were then sintered at 875 °C, 900 °C and 925 °C for 4 h in air.

The crystalline phase structure of these composite ceramics was analysed by X-ray diffraction (XRD: DX-2700, Haoyuan Co.) using Cu $K_\alpha$ radiation. XRD data were evaluated using Fullprof with the Rietveld profile refinement method. Microstructure was examined by scanning electron microscopy (SEM: JEOL, JSM-6490LV), and composition was studied by energy-dispersive X-ray spectroscopy (EDS). The microwave dielectric properties were determined via the Hakki−Coleman method and Agilent N5230A Network Analyser (300 MHz-20 GHz) [8]. The quality factor was investigated through the transmission cavity method. Transition temperature and shrinkage characteristics were analysed through a thermo-mechanical analyser (TMA: Mettler TMA/SDTA 2+), and the heating rate was 10 °C/min. The temperature coefficient of the resonant

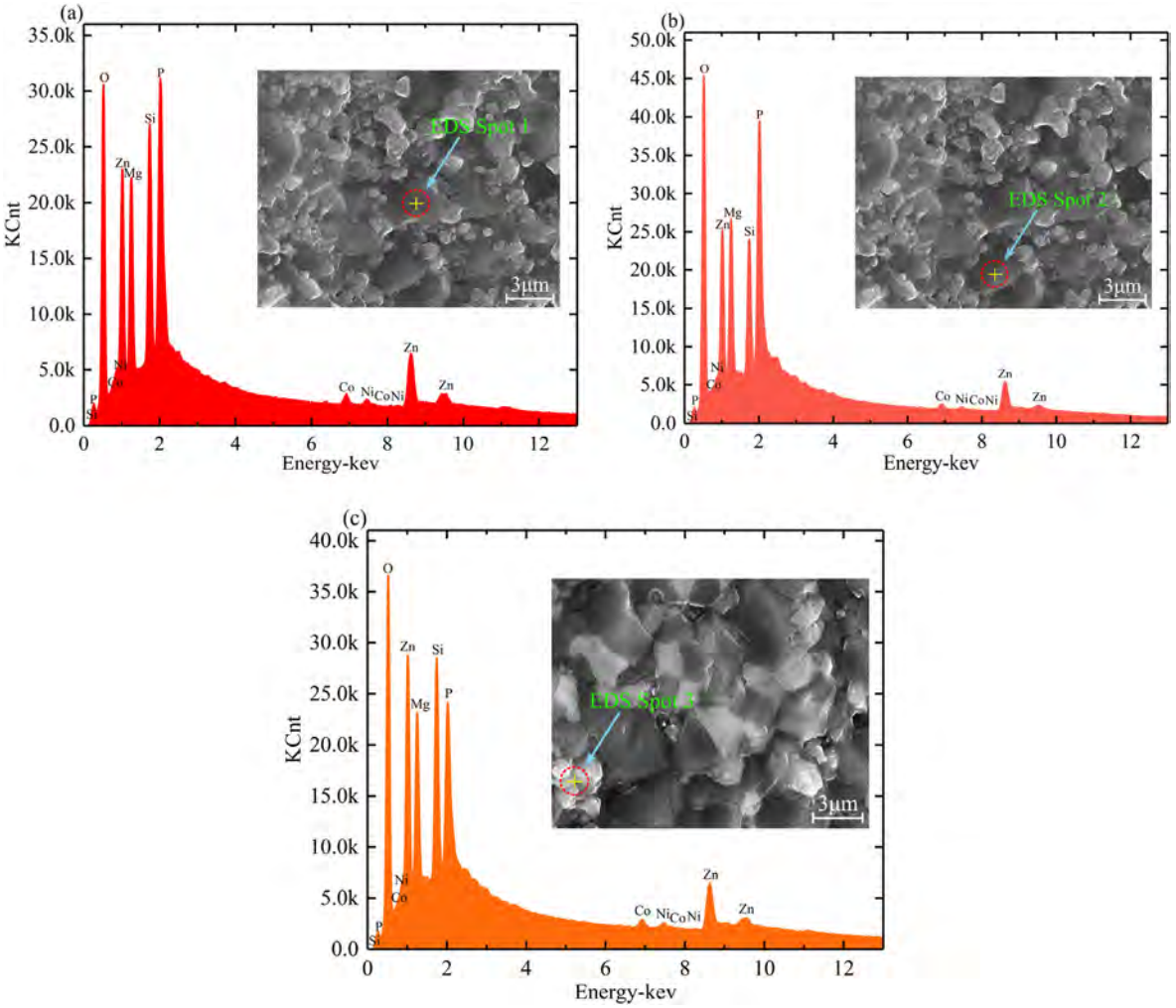


**Fig. 3.** EDS of 0.8LMNS+0.2LZCP (a−b) ceramic and 0.5LMNS+0.5LZCP (c) ceramic sintered at 900 °C (energy spectrum and tested area).

**Table 1**
EDS result (weight and atomic fraction) of spot1, spot2 and spot3.

| Element | Spot1 | | Spot2 | | Spot3 | |
|---|---|---|---|---|---|---|
| | Weight (%) | Atomic (%) | Weight (%) | Atomic (%) | Weight (%) | Atomic (%) |
| O K | 37.25 | 56.44 | 45.23 | 63.70 | 40.36 | 59.97 |
| Mg K | 12.71 | 12.67 | 12.75 | 11.82 | 13.40 | 13.10 |
| Si K | 9.97 | 8.61 | 6.65 | 5.33 | 10.55 | 8.93 |
| P K | 17.80 | 13.93 | 18.00 | 13.09 | 12.17 | 9.34 |
| Co K | 1.51 | 0.62 | 1.06 | 0.40 | 1.59 | 0.64 |
| Ni K | 0.56 | 0.23 | 0.61 | 0.24 | 1.18 | 0.48 |
| Zn K | 20.20 | 7.49 | 15.70 | 5.41 | 20.74 | 7.53 |

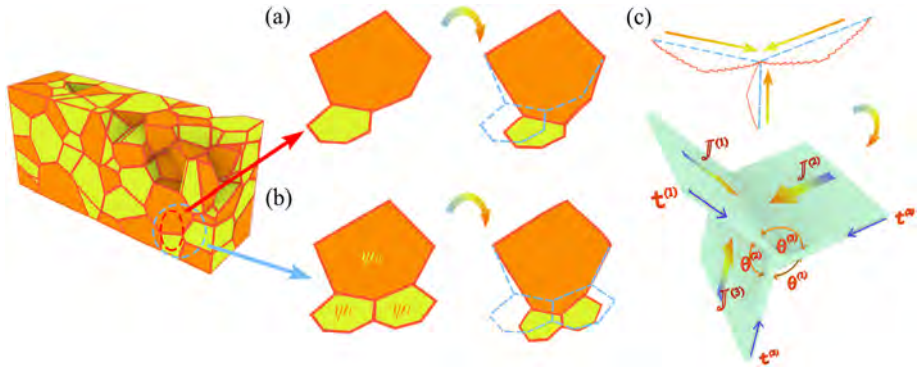


**Fig. 4.** Schematic of GB motion of biphase system (a), triple junctions motion of triphase system (b), relationship between the parameters from equation (4) (c); blue dashed lines in (a)–(c) denote the initial GB position. (For interpretation of the references to colour in this figure legend, the reader is referred to the Web version of this article).

frequency ($\tau_f$) of the ceramics was measured using the following formula [9].

$$\tau_f = \frac{f_T - f_0}{f_0(T - T_0)} \times 10^6 \quad (1)$$

where $f_T$ ($f_0$) is the resonant frequencies at $T = 80$ °C ($T_0 = 20$ °C). The bulk density of the sample was determined through the Archimedes method, and the relative densities were from the ratio of bulk densities and the theoretical densities. The theoretical $\tau_f$ and $\varepsilon_r$ value could be calculated using the mixture rule as follows [10,11].

$$\tau_f = v_a \times \tau_{fa} + v_b \times \tau_{fb} \quad (2)$$

$$\ln \varepsilon_r = v_a \ln \varepsilon_{ra} + v_b \ln \varepsilon_{rb} \quad (3)$$

where $\tau_{fa}$ ($\tau_{fb}$) and $\varepsilon_{ra}$ ($\varepsilon_{rb}$) are the temperature coefficient of the resonant frequency of a (b) and the dielectric constant of a (b); the volume fractions of different materials are $v_a$ and $v_b$.

## 3. Results and discussion

Fig. 1 presents the relative density (a), $\varepsilon_r$ (b), $Q \times f$ (c) and $\tau_f$ (d) of the (1-x)LMNS + xLZCP (x = 0.2–0.7) ceramics sintered at 875 °C-925 °C. All the dielectric properties were obtained at 16 GHz, which is the mean value of testing frequency (15.92–16.08 GHz). The curve of relative density is parabola like, and the maximum value is approximately 96.1% as x = 0.5 sintered at 900 °C. A moderate amount of LZCP ceramic addition could help increase the densification level at the fixed sintering temperature. However, further addition of LZCP ceramic deteriorated the densification level (over sintering) because the densification temperature of LZCP ceramic (850 °C) is lower than the sintering temperature of this study (900 °C). The dielectric constant ($\varepsilon_r$) of the composite ceramics decreases with increasing x value due to the relative low dielectric constant of LZCP ceramic ($\varepsilon_r = 5.78$ as x = 0.5). The measured $\varepsilon_r$ value of the ceramics is higher than the calculated one when x < 0.6, and the formation of the second phase ($Mg_2SiO_4$, discussed in the part of XRD) could explain this phenomenon. However, the calculated $\varepsilon_r$ value is larger than the experimental one when x = 0.7, and the non-ideal densification level could be one reason responsible for this discrepancy. The $Q \times f$ value increased with the x value and peaked at x = 0.5 (48,168 GHz at 16 GHz) and decreased. The variation tendency shown by the $Q \times f$ value is similar to that of the relative density value. The $Q \times f$ value of 0.5LMNS+0.5LZCP composite material is larger than the value of the separate one of our previous research, and the better densification of the former than the latter could explain this difference. For the $\tau_f$ value of the composite ceramics, the variation exhibits a monotonically decreasing trend due to the small $\tau_f$ value of LZCP ceramic. The subtle disparity between the measured and calculated $\tau_f$ values ($\tau_f = -44.7$ ppm/°C) is attributed to the compact samples. Fig. 1e shows the comparison of the dielectric properties and densification temperatures of various microwave dielectric ceramics with relative low $\varepsilon_r$ and high $Q \times f$ value [6,7,12–22]. With the addition of LZCP ceramic, the composite ceramic is equipped with excellent microwave dielectric properties, high $Q \times f$ value, low $\varepsilon_r$ and low densification temperature (approximately 900 °C) without sintering aids.

Fig. 2 manifests the SEM images of all samples. The microstructure property variation trend of the (1-x)LMNS + xLZCP ceramics sintered at different temperatures is regular and identical to the trend of the relative density. The large grains (blue circles) are surrounded by small grains (yellow circles) (Fig. 2a–d). The number of small grains decreases with when the x value increases, and uniform large grains are formed when x = 0.5 with a few of small grains. Further addition of LZCP ceramic leads to the appearance of trapped pores (pink circles), and grain boundaries melt due to over-

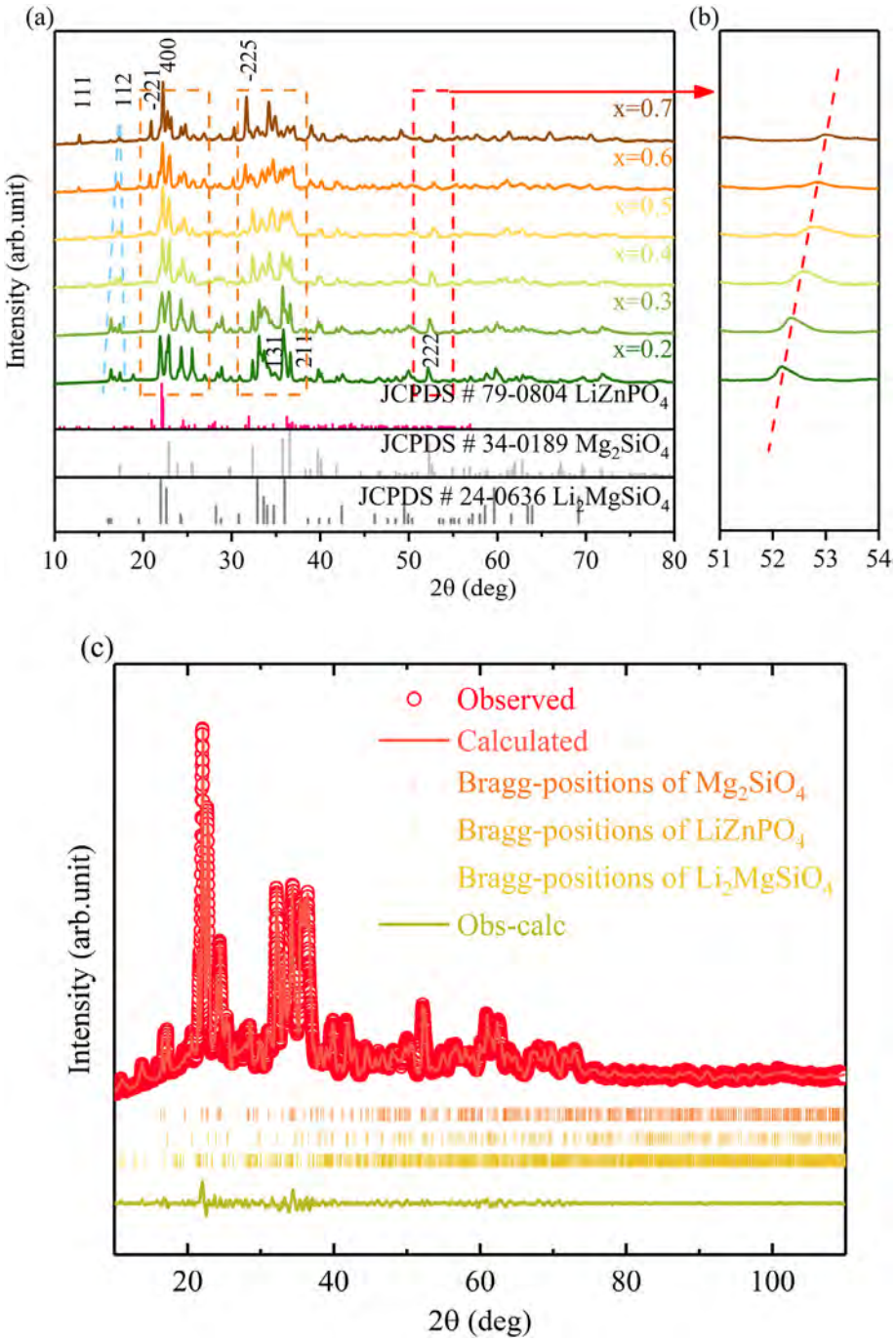


**Fig. 5.** XRD patterns of the (1-x)LMNS + xLZCP (x = 0.2–0.7) composite ceramics sintered at 900 °C (a); locally magnified peak profiles (b); Experimental (circles) and calculated (lines) XRD profiles for the 0.5LMNS+0.5LZCP ceramics sintered at 900 °C using Fullprof software (c).

sintering because the densification temperature of the LZCP ceramic is approximately 825 °C. The microstructure presented in Fig. 2d,g,h suggests that the sintering temperature of 900 °C is suitable for the 0.5LMNS+0.5LZCP composite ceramic to obtain a closely packed microstructure. Considering all the dominant factors for the extrinsic losses, including second phase, grain size, crystal boundaries, cracks, impurities and porosity, the reduction of the grain boundary should be taken into account for the first increment of $Q \times f$ value apart from the increased densification level [23–25]. Hence, the materials with highly compact and uniform crystal grains present a relatively high $Q \times f$ value. The formed pores and abnormal grain growth shown in the SEM images might cause the dielectric properties to deteriorate. EDS was conducted to identify the composition of the aimed region to confirm the component of small grains and large grains shown in SEM. The tested area and results are presented in Fig. 3 and Table 1, and all the marked grains consist of O, Mg, Si, P, Co, Ni and Zn (Li is too light to be checked). The molar ratio of P:Si is 13.93:8.61 for spot 1 and 13.09:5.33 for spot 2, indicating that the large grains should be the P-rich phase and the small grains should be the Si-rich phase. The molar ratio of P:Si is 9.34:8.93 for spot 3, demonstrating that the distribution of phosphate and silicate could be uniform in the small grains and the

**Table 2**
Refinement and lattice parameters of (1-x)LMNS + xLZCP (x = 0.2–0.7) ceramics sintered at 900 °C using Rietveld profile refinement method.

| Parameters | x = 0.2 | x = 0.3 | x = 0.4 | x = 0.5 | x = 0.6 | x = 0.7 |
|---|---|---|---|---|---|---|
| LMNS | | | | | | |
| *a* (Å) | 4.9889 | 4.9868 | 4.9850 | 4.9842 | 4.9835 | 4.9831 |
| *b* (Å) | 10.6805 | 10.6824 | 10.6838 | 10.6843 | 10.6851 | 10.6860 |
| *c* (Å) | 6.3117 | 6.3086 | 6.3069 | 6.3050 | 6.3035 | 6.3028 |
| *β* (°) | 90.1908 | 90.2662 | 90.3214 | 90.3743 | 90.4119 | 90.4401 |
| *V* (Å$^3$) | 336.3104 | 336.0618 | 335.8923 | 335.7510 | 335.6476 | 335.6105 |
| LZCP | | | | | | |
| *a* (Å) | 17.2851 | 17.2842 | 17.2831 | 17.2819 | 17.2792 | 17.2771 |
| *b* (Å) | 9.7468 | 9.7482 | 9.7493 | 9.7507 | 9.7518 | 9.7545 |
| *c* (Å) | 17.0747 | 17.0759 | 17.0772 | 17.0781 | 17.0793 | 17.0815 |
| *β* (°) | 110.9822 | 110.9798 | 110.9745 | 110.9689 | 110.9611 | 110.9524 |
| *V* (Å$^3$) | 2685.9043 | 2686.3822 | 2686.8141 | 2687.2557 | 2,687.4679 | 2,688.3879 |
| MS | | | | | | |
| *a* (Å) | 4.7533 | 4.7505 | 4.7485 | 4.7469 | 4.7451 | 4.7442 |
| *b* (Å) | 10.1994 | 10.1975 | 10.1961 | 10.1955 | 10.1948 | 10.1942 |
| *c* (Å) | 5.9832 | 5.9861 | 5.9886 | 5.9904 | 5.9916 | 5.9923 |
| *β* (°) | 90.00 | 90.00 | 90.00 | 90.00 | 90.00 | 90.00 |
| *V* (Å$^3$) | 290.0704 | 289.9860 | 289.9451 | 289.9175 | 289.8457 | 289.8075 |
| $R_p$ (%) | 10.39 | 10.61 | 9.53 | 9.27 | 10.78 | 11.08 |
| $R_{wp}$ (%) | 11.81 | 11.52 | 10.72 | 10.58 | 12.55 | 13.99 |
| $R_{exp}$ (%) | 7.96 | 8.12 | 7.54 | 7.84 | 8.63 | 9.54 |
| $\chi^2$ | 2.20 | 2.01 | 2.02 | 1.82 | 2.11 | 2.15 |

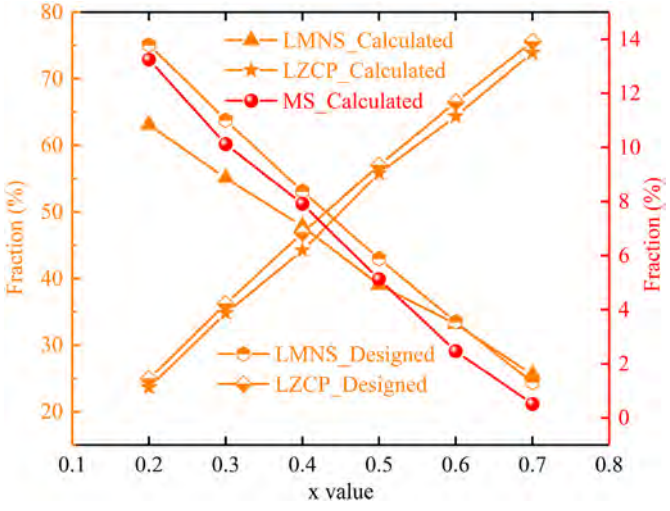


**Fig. 6.** Designed and calculated fraction of LMNS, LZCP and MS of the composite ceramics.

large grains when x = 0.5.

The sintering kinetics of GBs based on the disconnection model was proposed to explain the variation in grain size and grain composition, and the schematic is presented in Fig. 4 [26,27]. The following discussion is about the perfect process (without the emission and absorption of point defects or lattice dislocation) [28,29]. The grain growth and grain motion of the polycrystal material in this experiment can be divided into two aspects. The first is the GB motion of the biphase system (Fig. 4a), and the second is the triple junction (TJ) motion of the triphase system (Fig. 4b). Intrinsic GB mobility, including GB migration (perpendicular to GB) and GB sliding (parallel to GB), is a dominant thermal equilibrium character of GB motion at the subatomic scale. These two phenomena are always coupled as illustrated in Fig. 4a. According to the driving source, the GB migration can be divided into stress-driven GB migration and energy-jump-driven migration [30,31]. The increasing sintering temperature results in nucleation and gliding, and the shear strain will be gathered on both sides of GBs. Then, the shear stress is gathered under the increasing sintering temperature, and the phase on each side of GB belonging to 0.5LMNS+0.5LZCP ceramic glides away with the migration of GB. These factors could explain the phenomenon observed in Fig. 2(d), (g) and (h). The energy-jump-driven migration is attributed to the lower total free energy similar to the diffusion-induced GB migration [32–34]. If the free energy density (dominated by the eigen-property of materials, like crystal structure) of the upper grain ($\psi_u$) is smaller than that of lower grain ($\psi_l$), GB would migrate downwards to decrease the total system free energy (Fig. 4b). Considering the SEM and EDS results, the free energy density of P-rich grains may be lower than that of the Si-rich grains. Consequently, the grain has grown, and the amount of small grains has decreased as x values vary from 0.2 to 0.5 sintered at 900 °C (Fig. 2a–d).

Aside from GB, TJ, the node of GBs in the polycrystals, should be considered. The GBs are finite in practice due to the existence of TJs. In the disconnection model, the motion of GBs is a stepped motion, and nucleated disconnections will move to TJs. The corresponding schematic is presented in Fig. 4c. The annihilation and reaction of the disconnections near TJs enable TJ to move. The velocity of TJ could be quantified by the disconnection flux ($J^{(i)}$) from GB$^{(i)}$, the angle ($\theta^{(k)}$) between GB$^{(i)}$ and GB$^{(j)}$ and step height ($h^{(i)}$) as follows [35].

$$\mathbf{v}_{TJ} = \frac{2}{3}\left\{\left[\frac{J^{(3)}h^{(3)}}{Sin\theta^{(2)}} - \frac{J^{(2)}h^{(2)}}{Sin\theta^{(3)}}\right]\mathbf{t}^{(1)} + \left[\frac{J^{(1)}h^{(1)}}{Sin\theta^{(3)}} - \frac{J^{(3)}h^{(3)}}{Sin\theta^{(1)}}\right]\mathbf{t}^{(2)} + \left[\frac{J^{(2)}h^{(2)}}{Sin\theta^{(1)}} - \frac{J^{(1)}h^{(1)}}{Sin\theta^{(2)}}\right]\mathbf{t}^{(3)}\right\} \quad (4)$$

The growth of grain with GB$^{(2)}$ and GB$^{(3)}$ could be realized if the sum of the second and third terms in Equation (4) meet the two requirements: positive and larger than the first term (absolute value). Therefore, the values with vector along P-rich grain may play a dominant role in this experiment from the perspective of TJ motion. Generally, the infinite movement of TJ is difficult to infer considering the accumulation of Burgers vectors and the incompatible GB displacements at TJ. However, at a relatively high temperature, the disconnection mode with the lowest nucleation barrier is more than that at TJ, leading to the further movement of

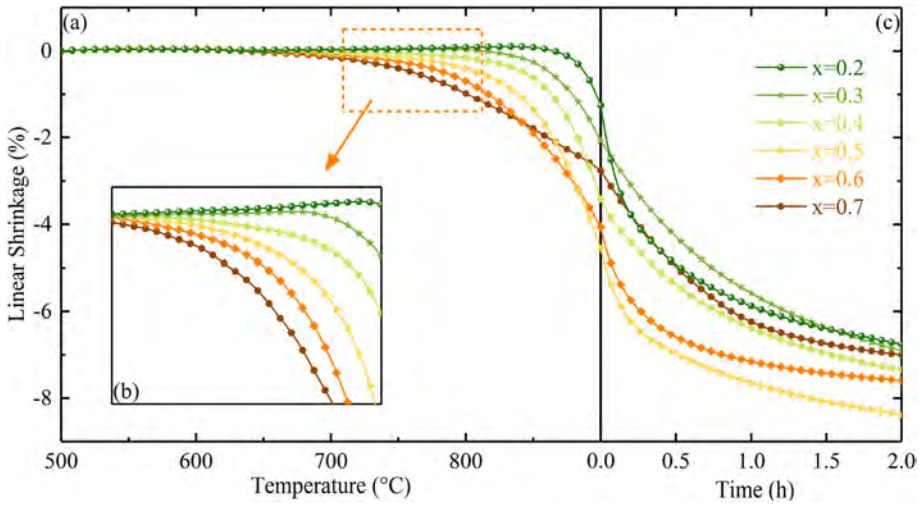


**Fig. 7.** Shrinkage curves of (1-x)LMNS + xLZCP (x = 0.2–0.7) composite ceramics as a function of sintering temperature and holding time.

TJ. These phenomena could further explain the grain growth of the 0.5LMNS+0.5LZCP composite ceramic sintered at different temperatures. However, the emission and absorption of point defects or lattice dislocation always exist in reality (imperfect process) [29]. Under the imperfect situation, point defect absorption and solute atom diffusion are the two typical causes of GB migration. The above discussion is based on the assumption that, for convenience, the original characteristics of the GB structure is maintained with or without point defect emission. However, the transformation of GB structure through diffusion induced recrystallization is possible [36,37]. Therefore, a more detailed study is needed in future work.

The XRD patterns of the (1-x)LMNS + xLZCP (x = 0.2–0.7) ceramics sintered at 900 °C for 4 h are shown in Fig. 5(a–b). These patterns show that the diffraction peaks of all samples can be well indexed in three standard patterns: $LiZnPO_4$ (JCPDS # 79-0804, *Cc* No.9), $Mg_2SiO_4$ (JCPDS # 34-0189, *Pmnb* No.62) and $Li_2MgSiO_4$ (JCPDS # 24-0636, $P2_1/n$ No.14). The diffraction peak intensity varies with increasing x value. The peak intensity of $Mg_2SiO_4$ (MS) and $Li_2MgSiO_4$ ceramics decreases gradually but that of the $LiZnPO_4$ ceramic increases. This variation could be observed in the (111) peak, (112) peak and the red and orange dotted box. The (222) peak of $Mg_2SiO_4$ pattern moves to a high angle slightly with increasing x value. This phenomenon is attributed to the similar radii of the $Mg^{2+}$ (0.57 Å) and the $Zn^{2+}$ (0.60 Å), resulting in the non-negligible replacement ($Zn^{2+}$ to $Mg^{2+}$) when the $Zn^{2+}$ concentration is augmented [38]. A lattice distortion could occur due to the different theoretical ionic polarisability of $Mg^{2+}$ (1.32 $Å^3$) and $Zn^{2+}$ (2.04 $Å^3$) [39]. Therefore, LMNS ceramic formation in the composite system is insufficient at relative low sintering temperatures, and a large amount of LZCP ceramic addition could promote LMNS ceramic formation.

The refinements were conducted using Fullprof software to investigate the crystal structure details of the composite ceramics (Fig. 5c, Table 2). The fitted curves and the experimental ones are almost the same, and the Bragg positions of all phases match the indexed peaks well. All the fitting parameters are acceptable. The cell volumes of LMNS and MS ceramic decrease as the x value increases, and that of the LZCP ceramic exhibits an increasing trend. This tendency should be ascribed to the varying ion concentrations of $Zn^{2+}$ and $Mg^{2+}$ with increasing x value. The mutual substitution level is changed, and the difference in ionic polarisability may result in lattice distortion. Fig. 6 presents the designed and calculated fraction value of LMNS, LZCP and MS ceramics of the composite materials. The variation tendency of the designed and calculated value is generally consistent except for the existence of the second phase (MS). The MS ceramic content shows a decreasing tendency, which is consistent with the XRD patterns and is attributed to the reduced designed fraction of the LMNS ceramic. Considering that the dielectric properties of MS are $\varepsilon_r$ = 6.9, $\tau_f$ = −67 ppm/°C, and $Q \times f$ = 240,000 GHz, the decreasing MS phase could also lead to the decreasing $\varepsilon_r$ and $Q \times f$ value [40]. Therefore, the presence of MS is another factor that contributes to the discrepancy between the measured and calculated $\varepsilon_r/\tau_f$ values. In addition, the second phase (MS) plays a more important role than the relative density in the $\varepsilon_r$ value of the (1-x)LMNS + xLZCP ceramics when x < 0.6. Furthermore, MS ceramic (high $Q \times f$ value) formation could explain the larger peak $Q \times f$ value of the composite materials than those of the LMNS and LZCP ceramics.

The shrinkage behaviour of the materials was determined by TMA as a function of sintering temperature and holding time (Fig. 7). The shrinkage onset of (1-x)LMNS + *x*LZCP ceramics exhibited a decreasing trend with increasing *x* value (650 °C-850 °C). This result is attributed to the relative low phase-forming temperature of LZCP ceramic compared with that of the LMNS ceramic. Therefore, onset point of the sample with high LZCP content can be adjusted to a relatively low temperature. The final shrinkage value of the 0.5LMNS+0.5LZCP composite ceramic sintered at 900 °C is larger than those of others, and the shrinkage result is nearly consistent with that of the relative density. Considering the relative density value, microstructure and shrinkage curve, the full densification could be reached with 0.5LZCP ceramic sintered at 900 °C.

## 4. Conclusion

Low temperature-sintering composite ceramics without sintering aids were synthesised through solid-state reaction. The sintering kinetics of grains and the effects of microstructure on the microwave dielectric properties were investigated. The LZCP ceramic could promote grain growth due to the difference of shear stress and the free energy density of the Si- and P-rich phases on both sides of GB. The shrinkage onset point of the composite ceramics was adjusted to reach full densification at 900 °C. The synthesised material exhibits excellent microwave dielectric properties at $x$ = 0.5 with uniform grains and compact microstructure, $\varepsilon_r$ = 5.78, $Q \times f$ = 48,168 GHz at 16 GHz, $\tau_f$ = −44.7 ppm/

°C and relative density = 96.1%. Therefore, mixing the LZCP ceramic and LMNS ceramic is a feasible synthesis method for microwave dielectric materials with excellent sintering and dielectric properties.

## Declaration of competing interest

There is something that I want to declare on behalf of my co-authors.1.

There is no conflict of interest in the submission of this manuscript and all authors have approved to publish this paper.2.

The research work that this manuscript described was original, which has not been published previously and not under consideration for publication on elsewhere.

## CRediT authorship contribution statement

**Rui Peng:** Conceptualization, Methodology, Software, Investigation, Writing - original draft. **Yuanxun Li:** Funding acquisition, Writing - review & editing. **Yongcheng Lu:** Validation, Formal analysis, Visualization, Software. **Yanru Yun:** Validation, Formal analysis, Visualization, Supervision. **Wei Du:** Supervision, Data curation. **Zhihua Tao:** Funding acquisition, Writing - review & editing. **Bin Liao:** Funding acquisition, Writing - review & editing.

## Acknowledgements

This work was supported by the Jiangxi Innovative Talent Program, Jiangxi Guochuang & UESTC Joint R & D Center Program (Grant No. H04W190371), and National Key Research and Development Project (Grant No. 2017YFB0406300).

## References

[1] Y. Lai, X. Tang, X. Huang, H. Zhang, X. Liang, J. Li, H. Su, Phase composition, crystal structure and microwave dielectric properties of Mg2−xCuxSiO4 ceramics, J. Eur. Ceram. Soc. 38 (2018) 1508−1516.
[2] W. Lei, Z.-Y. Zou, Z.-H. Chen, B. Ullah, A. Zeb, X.-K. Lan, W.-Z. Lu, G.-F. Fan, X.-H. Wang, X.-C. Wang, Controllable τf value of barium silicate microwave dielectric ceramics with different Ba/Si ratios, J. Am. Ceram. Soc. 101 (2018) 25−30.
[3] Y. Lai, H. Su, G. Wang, X. Tang, X. Liang, X. Huang, Y. Li, H. Zhang, C. Ye, X.R. Wang, Improved microwave dielectric properties of CaMgSi2O6 ceramics through CuO doping, J. Alloys Compd. 772 (2019) 40−48.
[4] W. Lei, W.-Z. Lu, J.-H. Zhu, F. Liang, D. Liu, Modification of ZnAl2O4-based low-permittivity microwave dielectric ceramics by adding 2MO−TiO2(M=Co, Mg, and Mn), J. Am. Ceram. Soc. 91 (2008) 1958−1961.
[5] H.-H. Guo, D. Zhou, L.-X. Pang, Z.-M. Qi, Microwave dielectric properties of low firing temperature stable scheelite structured (Ca, Bi)(Mo, V)O4 solid solution ceramics for LTCC applications, J. Eur. Ceram. Soc. 39 (2019) 2365−2373.
[6] R. Peng, H. Su, D. An, Y. Lu, Z. Tao, D. Chen, L. Shi, Y. Li, The sintering and dielectric properties modification of Li2MgSiO4 ceramic with Ni2+-ion doping based on calculation and experiment, J. Mater. Res. Technol. (2019), https://doi.org/10.1016/j.jmrt.2019.11.061.
[7] R. Peng, Y. Li, G. Yu, Y. Lu, S. Li, Effect of Co2+ substitution on the microwave dielectric properties of LiZnPO4 ceramics, J. Electron. Mater. 47 (2018) 7281−7287.
[8] B.W. Hakki, P.D. Coleman, A dielectric resonator method of measuring inductive capacities in the millimeter range, Ire Trans. Microw. Theory Tech. 8 (2003) 402−410.
[9] C. Zhang, R. Zuo, J. Zhang, Y. Wang, J. Jones, Structure-dependent microwave dielectric properties and middle-temperature sintering of forsterite (Mg1-xNix)2SiO4 ceramics, J. Am. Ceram. Soc. 98 (2015) 702−710.
[10] Y. Lv, R. Zuo, Y. Cheng, C. Zhang, P. Davies, Low-temperature sinterable (1−x)Ba3(VO4)2-xLiMg0.9Zn0.1PO4 microwave dielectric ceramics, J. Am. Ceram. Soc. 96 (2013) 3862−3867.
[11] Y.-N. Wang, Y.-C. Chen, S.-L. Yao, C.-Y. Wu, Microwave dielectric properties of neodymium tin oxide, Ceram. Int. 40 (2014) 2641−2645.
[12] X. Du, H. Su, H. Zhang, Y. Jing, Z. Zhou, G. Gan, X. Tang, Effects of Li-ion substitution on the microwave dielectric properties of low-temperature sintered ceramics with nominal composition Li2xMg2−xSiO4, Ceram. Int. 44 (2018) 2300−2303.
[13] C.C. Xia, D.H. Jiang, G.H. Chen, Y. Luo, B. Li, C.L. Yuan, C.R. Zhou, Microwave dielectric ceramic of LiZnPO4 for LTCC applications, J. Mater. Sci. Mater. Electron. 28 (2017) 12026−12031.
[14] S. George, P.S. Anjana, V.N. Deepu, P. Mohanan, M.T. Sebastian, Low-temperature sintering and microwave dielectric properties of Li2MgSiO4 ceramics, J. Am. Ceram. Soc. 92 (2009) 1244−1249.
[15] T. Joseph, M.T. Sebastian, H. Sreemoolanadhan, V.K. Sree Nageswari, Effect of glass addition on the microwave dielectric properties of CaMgSi2O6 ceramics, Int. J. Appl. Ceram. Technol. 7 (2009) E98−E106.
[16] T. Guo, Y. Li, O. Wahyudi, S. Chen, X. Wang, J. Chen, Microwave dielectric properties of AZn2(PO4)2 (A=Sr, Ba) ceramics, Ferroelectrics 492 (2016) 91−102.
[17] G. Dou, D. Zhou, S. Gong, M. Guo, Low temperature sintering and microwave dielectric properties of Li2ZnSiO4 ceramics with ZB glass, J. Mater. Sci. Mater. Electron. 24 (2012) 1601−1607.
[18] E.S. Kim, B.S. Chun, R. Freer, R.J. Cernik, Effects of packing fraction and bond valence on microwave dielectric properties of A2+B6+O4 (A2+: Ca, Pb, Ba; B6+: Mo, W) ceramics, J. Eur. Ceram. Soc. 30 (2010) 1731−1736.
[19] U. Došler, M.M. Kržmanc, D. Suvorov, The synthesis and microwave dielectric properties of Mg3B2O6 and Mg2B2O5 ceramics, J. Eur. Ceram. Soc. 30 (2010) 413−418.
[20] Z. Cheng, X. Hu, Y. Li, Z. Ling, N. Alford, Fabrication and microwave dielectric properties of Mg2SiO4-LiMgPO4-TiO2 composite ceramics, J. Am. Ceram. Soc. 99 (2016) 2688−2692.
[21] Z. Zhou, H. Su, X. Tang, H. Zhang, F. Xu, S. Zhang, Y. Jing, Microwave dielectric properties of LBBS glass added (Zn0.95Co0.05)2SiO4 for LTCC technology, Ceram. Int. 42 (2016) 11161−11164.
[22] T.S. Sasikala, C. Pavithran, M.T. Sebastian, Effect of lithium magnesium zinc borosilicate glass addition on densification temperature and dielectric properties of Mg2SiO4 ceramics, J. Mater. Sci. Mater. Electron. 21 (2009) 141−144.
[23] M. Guo, G. Dou, S. Gong, D. Zhou, Low-temperature sintered MgWO4−CaTiO3 ceramics with near-zero temperature coefficient of resonant frequency, J. Eur. Ceram. Soc. 32 (2012) 883−890.
[24] V.L. Gurevich, A.K. Tagantsev, Intrinsic dielectric loss in crystals, Adv. Phys. 40 (1991) 719−767.
[25] S.J. Penn, N.M. Alford, A. Templeton, X. Wang, M. Xu, M. Reece, K. Schrapel, Effect of porosity and grain size on the microwave dielectric properties of sintered alumina, J. Am. Ceram. Soc. 80 (1997) 1885−1888.
[26] J.P. Hirth, R.C. Pond, J. Lothe, Spacing defects and disconnections in grain boundaries, Acta Mater. 55 (2007) 5428−5437.
[27] R.W. Balluffi, A. Brokman, A.H. King, CSL/DSC Lattice model for general crystalcrystal boundaries and their line defects, Acta Metall. 30 (1982) 1453−1470.
[28] A.P. Sutton, Interfaces in crystalline materials, Monogr. Phy. Chem. Mater. (1995) 414−423.
[29] R.W. Balluffi, S. Allen, W.C. Carter, Kinetics of Materials, John Wiley & Sons, 2005.
[30] C.H. Li, E.H. Edwards, J. Washburn, E.R. Parker, Stress-induced movement of crystal boundaries, Acta Metall. 1 (1953) 223−229.
[31] K.G. Janssens, D. Olmsted, E.A. Holm, S.M. Foiles, S.J. Plimpton, P.M. Derlet, Computing the mobility of grain boundaries, Nat. Mater. 5 (2006) 124.
[32] F. Rhines, A. Montgomery, A new type of structure in the α-copper-zinc alloys, Nature 141 (1938) 413.
[33] B. Langelier, S.Y. Persaud, A. Korinek, T. Casagrande, R.C. Newman, G.A. Botton, Effects of boundary migration and pinning particles on intergranular oxidation revealed by 2D and 3D analytical electron microscopy, Acta Mater. 131 (2017) 280−295.
[34] D.L. Beke, Y. Kaganovskii, G.L. Katona, Interdiffusion along grain boundaries − diffusion induced grain boundary migration, low temperature homogenization and reactions in nanostructured thin films, Prog. Mater. Sci. 98 (2018) 625−674.
[35] A. Sisanbaev, R. Valiev, The effect of triple junction type on grain-boundary sliding and accomodation in aluminium tricrystals, Acta Metall. Mater. 40 (1992) 3349−3356.
[36] M. Kasprzak, D. Baither, G. Schmitz, Diffusion-induced recrystallization in nickel/palladium multilayers, Acta Mater. 59 (2011) 1734−1741.
[37] F. Hartung, G. Schmitz, Interdiffusion and reaction of metals: the influence and relaxation of mismatch-induced stress, Phys. Rev. B 64 (2001), 245418.
[38] R.D. Shannon, Revised effective ionic radii and systematic studies of interatomic distances in halides and chalcogenides, Acta Crystallogr. 32 (1976) 751−767.
[39] R.D. Shannon, Dielectric polarizabilities of ions in oxides and fluorides, J. Appl. Phys. 73 (1993) 348−366.
[40] T. Tsunooka, M. Androu, Y. Higashida, H. Sugiura, H. Ohsato, Effects of TiO2 on sinterability and dielectric properties of high-Q forsterite ceramics, J. Eur. Ceram. Soc. 23 (2003) 2573−2578.